

The Evolving Temperature Field in a 1 m Methanol Pool Fire

Journal of Fire Sciences, Volume 39 (4), 309-323 (2021)

Jian Chen,¹ Kunhyuk Sung,² Zhigang Wang,³ Wai Cheong Tam,² Ki Yong Lee,⁴ Anthony Hamins^{2,5}

1. Center for Offshore Engineering and Safety Technology, China University of Petroleum (East China), Qingdao, China
2. National Institute of Standards and Technology, Gaithersburg, MD 20899 USA
3. State Grid Electric Power Research Institute, Nanjing, China
4. Andong National University, Andong, South Korea
5. corresponding author: anthony.hamins@nist.gov

ABSTRACT

Thin filament pyrometry is used to measure the time-varying temperature field in a 1 m methanol pool fire. A digital camera with optical filters and zoom lens recorded the emission intensity of an array of 12 μm Silicon-Carbide filaments oriented horizontally at various heights across the steadily burning pool fire. A 50 μm diameter thermocouple measured the temperature at locations corresponding to the filament positions. A correlation was developed between the local probability density functions of the thermocouple time series measurements corrected for radiation and thermal inertia effects and the camera grayscale pixel intensity of the filaments. A regression analysis yields the local mean temperature and its variance. The time series of the temperature field is transformed into average values during consecutive phases of the fire's puffing cycle, providing quantitative insight into the complex and dynamic structure of a turbulent fire.

KEYWORDS: methanol; pool fires, thin filament pyrometry; temperature field measurements

1. BACKGROUND

Pool fires are a fundamental type of combustion phenomena in which the fuel surface is flat and horizontal, providing a simple system with well-defined boundary conditions to test models and further the understanding of fire phenomena. Although many studies have been reported on the structure and dynamics of pool fires,^{1,2,3} none to our knowledge have reported on time-dependent measurements of the entire temperature field and presented those results as the average gas temperature field during consecutive phases of a fire's puffing cycle. The objective of this study is to better understand the complex structure of a large pool fire by quantifying the transient temperature field during each of the phases that constitute the fire's puffing cycle.

Typical fire model validation studies generally consider time-averaged point measurements – even if many simultaneous local measurements are available. Yet, point by point comparisons of mean values may mask large-scale flow field features. Thin filament pyrometry (TFP) offers relatively fast time response, high resolution, temperature measurements conducted over an entire flow field.⁴ Hariharan measured the temperature in a blue fire whirl above a 20 cm diameter pool of burning heptane, using TFP calibrated by fine wire thermocouples.^{5,6} Pitts used TFP to characterize the structure of 5 cm diameter acoustically phase-locked flickering methane-air diffusion flames.⁷ More recently, Wang et al. measured the mean and transient thermal structure of a steadily burning 0.3 m diameter methanol pool fire using TFP and found a Gaussian shaped distribution of large scale puffing frequencies characterizing the fire flow field.⁸ They report on the instantaneous temperature fields during sequential phases of the puffing fire, but consider only those cycles that occurred with a period of about 0.37 s, which is the dominant frequency, occurring about 60 % of the time. Puffing cycles that were not the dominant frequency were not considered, neglecting a significant fraction of the time series data. Here, we extend the work of Ref. [8] by considering the entire time series of data over the entire flow field of a much larger fire, 1 m in diameter, and attempt to improve the characterization of the time series of the local temperature and its variance. A 1 m diameter pool fire burning methanol (CH₃OH) is selected for study. Methanol was selected as fuel since its flames are blue and free of carbonaceous soot. This condition is advantageous for application of TFP methods as background radiative emission is negligible, which otherwise would obfuscate interpretation of the filament emission. Since blackbody emissions from soot are absent in methanol pool fires, the heat feedback to the surface of the pool, and consequently, its mass burning rate, is lower than hydrocarbon fires that have both gaseous and particulate radiative emission. This fire was also selected because the results complement previous studies that characterize the global and local properties of this fire, including the fire heat release rate, mass burning rate, radiative fraction, time-averaged temperature field, and heat flux to targets some distance from the fire.^{9,10}

2. EXPERIMENTAL METHOD

Experiments were conducted under a 6.0 m exhaust hood. Figure 1 shows a schematic of the experimental apparatus.

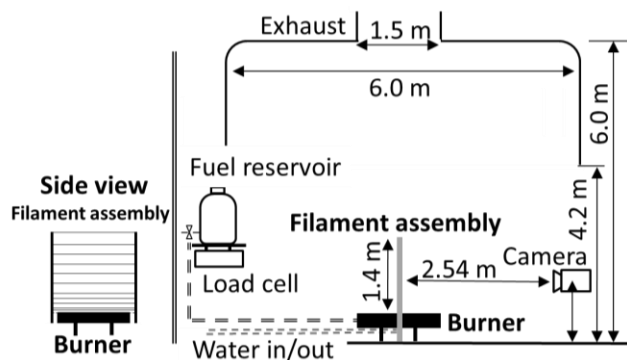


Figure 1 Drawing of the experimental apparatus

2.1 Burner and Exhaust

The fuel pan was placed in the open under a round 1.5 m diameter exhaust inlet located 6 m above the floor. The exhaust hood was 6 m by 6 m with skirts 4.2 m above the floor. Effects of ambient convective currents on the fire was minimized by closing supply lab air vents. The exhaust flow was about 4 kg/s.

A circular pan with an inner diameter (D) of $1.006 \text{ m} \pm 0.002 \text{ m}$, a depth of 0.15 m, and a wall thickness of 0.0016 m held the liquid methanol. The burner rim was located 0.5 m above the floor. Methanol purity was 99.99 % by mass and its density was 792.7 kg/m^3 at $20 \text{ }^\circ\text{C}$, according to the supplier. The bottom of the burner had a water-cooling section with thermocouples monitoring the water inlet and outlet temperatures. The water flow rate was about $57 \text{ L/min} \pm 1 \text{ L/min}$, ensuring that the bottom of the burner was maintained at a near constant temperature ($17 \text{ }^\circ\text{C} \pm 3 \text{ }^\circ\text{C}$).

Fuel to the burner was gravity fed from a reservoir on a mass load cell monitored by a data acquisition system. The fuel level was maintained 1 cm below the burner rim by regulating the fuel supply from the reservoir to the burner. The level was verified by visually observing the tip of a sharpened pointer that formed a barely discernable dimple on the fuel surface. A camera with optical zoom focused on the pointer, allowing observation of the fuel level. The mass burning rate was measured as $12.8 \text{ g/s} \pm 0.9 \text{ g/s}$ corresponding to an ideal heat release rate of $254 \text{ kW} \pm 19 \text{ kW}$. As expected, the heat release rate from oxygen consumption calorimetry was similar, measured as $256 \text{ kW} \pm 45 \text{ kW}$.^{9,10}

2.2 Thermocouple Measurements

A $50 \text{ }\mu\text{m}$ diameter, bare-bead, Type S (Pt-10% Rh/Pt) thermocouple mounted on a 50 cm long, 3 mm outer diameter, ceramic tube with two holes was used to calibrate the TFP measurement. The thermocouple (TC) and filament measurements were independently conducted. A precision translation stage moved the thermocouple through the flame. Figure 2 shows the thermocouple temperature measurement locations in the fire. The measured signal was acquired at a sampling rate of 60 Hz for 120 s, which represents about 170 flame puffing cycles..^{8,10} The temperature was typically measured three times at each location and always at least two times.

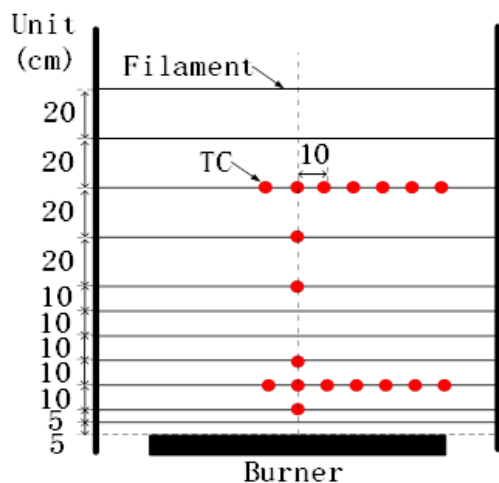


Figure 2. Locations in the fire where thermocouple (TC) and filament measurements were made.

The thermocouple bead was approximately spherical (eccentricity of 0.97) with a diameter of about $150\ \mu\text{m}$.^{9,10} The time series of the thermocouple (TC) temperature measurements were corrected for radiative loss and thermal inertia effects, considering an energy balance at the thermocouple bead.^{9,10} The temperature-dependent gas properties are taken as those of air and the temperature-dependent thermophysical properties of platinum are considered.^{11,12} The Fire Dynamics Simulator¹³ was used to simulate the local gas velocity, allowing estimation of the average local Reynolds number used in the thermal inertia correction. The peak mean gas velocity calculated by the FDS simulation was compared with Heskestad's plume model,¹⁴ which yielded similar results.^{9,10} In any case, the sensitivity of the thermal inertia temperature correction to the value of the local velocity was relatively small ($<5\ \text{K}$).^{9,10} The magnitude of the relative uncertainty of the local, instantaneous, gas temperature varied with the measured bead temperature, fire conditions (Re , Pr), and the rate of change of the time-varying temperature. Details of the gas temperature measurement and the uncertainty analysis are given in Refs. [9,10]

2.3 Thin Filament Pyrometry/Camera System

The local gas temperature was determined from the measured filament intensity. An array of $12\ \mu\text{m}$ diameter Silicon-Carbide (SiC) filaments (Hi-Nicalon Type S manufactured by Nippon Carbon Co.)* Their composition and characteristics have been previously described.¹⁵ The filaments were packaged in a bundle of 500 units encased in a polyvinyl acetate coating. Baking the bundle for 6 hours at $430\ ^\circ\text{C}$ removed the coating and allowed separation of individual filaments. The filaments were cut to approximately 1.4 m length. Each end was attached to string using a fast-drying cyanoacrylate liquid adhesive. Eleven filaments were aligned in a plane, parallel to each other; one above the other at 11 heights ($H=5\ \text{cm}$, $10\ \text{cm}$, $20\ \text{cm}$, $30\ \text{cm}$, $40\ \text{cm}$, $50\ \text{cm}$, $60\ \text{cm}$, $80\ \text{cm}$, $100\ \text{cm}$, $120\ \text{cm}$, $140\ \text{cm}$) above the burner rim on the pool centerline (see Figure 2). Each filament was stretched about 1.2 m between the posts of the filament assembly (see Figure 1), which was composed of modular extruded aluminum structural framing, and had wheels that ran on a track, allowing the assembly to be readily inserted and removed from the fire. For typical positions in this pool fire, the filament time response is estimated to be about 3 ms and has little effect on the measurement.^{16,17} Fire simulations of the 1 m methanol pool fire using the Fire

* Certain commercial entities, equipment, or materials may be identified in this document in order to describe an experimental procedure or concept adequately. Such identification is not intended to imply recommendation or endorsement by the National Institute of Standards and Technology, nor is it intended to imply that the entities, materials, or equipment are necessarily the best available for the purpose.

Dynamics Simulator¹³ showed that such a fast instrument time response can follow changes in the thermal field of the methanol fire. Because of the low thermal conductivity and the large convective heat transfer at the filament surface, broadening of the temperature distribution due to heat conduction is restricted to a small region near the hot surface. Heat conduction along the filament is estimated to be important over distances on the order of 100 μm , and the spatial resolution of the measurement is not limited by this factor.¹⁵

A Nikon 500D single lens reflex digital camera, similar to that used in previous studies, was fitted with optical filters and a zoom lens to record the filament emission intensity.^{5,6,8} Its pixel-to-pixel uniformity and other performance features make it suitable for thin filament pyrometry (TFP).⁸ The effects of lenses were investigated to optimize the signal. Based on previous TFP studies, several optical filters were tested to determine their effectiveness for TFP with methanol fires, including BG26, BG7, neutral density, and near-Infrared filters. The 3 mm thick, 50 \times 50 mm, Schott BG 26, blue filter in front of the lens was found to help improve the thin filament pyrometry signal to noise ratio. The grayscale pixel intensity was 8 bit in red (R), green (G), and blue (B).

Camera settings were adjusted to optimize the signal. Experiments collected 300 s of 29.97 Hz video at 4K Ultra High Definition (2160 \times 3840 pixels). Setting the zoom to 24 mm imaged the 100 cm by 140 cm high-temperature field. During the experiment, the F number was set to 2.8 and the shutter speed to 1/60 s. The ISO was adjusted to 400 to avoid pixel saturation. About 9000 frames were used in the analysis, which represented >400 cycles of the puffing fire. The camera focused on the filament array 2.54 m away. One pixel corresponded to about $\frac{1}{2}$ mm or about 40 times the 12 μm filament diameter.

Camera images were analyzed using MATLAB. The RGB pixel intensities were extracted and converted to grayscale as a weighted average of RGB values equal to $(0.2989R + 0.5870G + 0.1140B)$ following Ref. [18]. The results were multiplied by 2^8 as part of the calculation procedure such that the maximum pixel intensity was 65 535 ($2^{16} - 1$). Previous work showed that similar results were obtained using a TIFF format, rather than video mode and that the pixel sensitivity over the entire sensor was uniform to better than 0.5 %, which did not appreciably impact the temperature determination.⁸ Filament intensity was determined using the sum of grayscale values of several pixels perpendicular to the filament in either direction following Ref. [5]. The recorded camera image of the heated fiber is broad as previously reported due to “bleeding” of the image intensity from one pixel to its neighbors.^{5,6} Some amount of vertical motion of the filaments was also noticeable. It was observed that the sum of the filament intensity was invariant when integrating seven pixels across its width, so the maximum intensity was 450 000 theoretically (that is, seven times 65 535). The maximum measured intensity was about 350000. To ensure linearity, camera exposure conditions were selected such that the fiber images were bright, but did not saturate any pixel in any color plane at any time during the measurement. Saturation at any moment would have cut-off the signal, precluding accurate quantification of the high end of the temperature range.

2.4 Thin Filament Pyrometry (TFP) Calibration

The TFP calibration strategy employed the notion that at any fire location, the thermocouple and filament must experience the same thermal conditions, such that the probability density functions (PDFs) of the signals are positively correlated. By considering the PDFs, calibration curves relating the thermocouple (TC) temperature and the filament intensity were obtained. Since the filament intensity signal was only observable when the local temperature was sufficiently high, flame locations with the highest fractional probability of signal above background (P) were selected to construct the calibration. The experiment was repeated many times to optimize the dynamic range of the camera settings. The experiment was repeated once using the optimized camera settings. The PDFs of filament intensity and the corrected gas temperature were broken into 200 bins, with the average of each of the bins used to construct the calibration curve. Each bin has a certain probability of occurrence. The

idea is that the largest ½ % of occurrences of measured flame temperature in the PDF correspond to the largest ½ % of occurrences of measured filament intensities, the next largest ½ % of flame temperatures correspond to the next highest ½ % of filament emission intensities, and so on. The calibration curve was influenced by many factors, such as differences in background lighting, camera settings, or even ambient conditions that could affect camera sensitivity or background.

2.5 Experimental Procedure

Steady-state burning conditions were established before measurements were initiated by allowing a 10 min warm-up period. The fuel surface was maintained 10 mm below the burner rim. The burner bottom was water-cooled. A load cell monitored the fuel mass in the reservoir.⁹ To minimize the effect of water accumulation in the fuel pool due to back diffusion from the gas phase leading to condensation in the pool, fresh fuel was used for each experiment.

3. RESULTS AND DISCUSSION

3.1 Thermocouple Temperature and Filament Intensity

Figure 3 shows an over-exposed snapshot of the pulsing methanol fire with filaments mounted above the center of the burner. This low Froude number fire has large periodic vortical structures that lead to coherent puffing. For the TFP measurements, the camera conditions were adjusted so background flames were hardly visible.

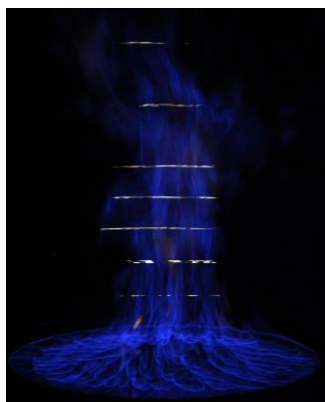


Figure 3 Over-exposed image of glowing filaments above central plane of the methanol fire

The filament grayscale intensity is a function of position and time. Figure 4 shows 300 consecutive frames (every 0.033 s) composing a 10 s time series of filament intensity at one location ($H=30$ cm, $R=20$ cm), which is in the flapping region of the puffing fire, where the high temperature reaction zone periodically swings back and forth. Analysis of the filament intensity was used to characterize the fire's puffing frequencies.

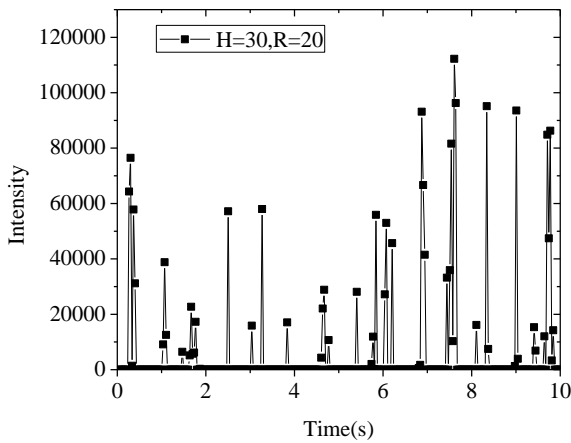


Figure 4 Time series of intensity measured on the filament at $H=30$ cm, $R=20$ cm, where H is the distance relative to the burner and R is the distance from the pool center

Using the maximum intensities as a reference to indicate the start of a puffing cycle, a counting procedure was used to determine the probability distribution of the periodicity of a fire pulsation cycle. Figure 5 shows that the distribution roughly follows a Gaussian in shape with a mean period of 21.3 frames ± 3.9 frames (0.71 s ± 0.13 s, corresponding to a frequency of 1.41 Hz) with a fractional probability of about 0.18 . Fast Fourier Transform (FFT) of the time series of the thermocouple and silicon carbide fiber TFP signal was considered at several positions – high and low in the fire; nearly the same dominant frequency was obtained with a value of approximately 1.39 Hz. This value represents the average frequency of the large scale vortical structures that roll into the fire and are convected upwards due to buoyancy, influencing the dynamics of the entire flow field. Additional frequencies occur, but the influence of the dominant frequency is evident throughout the flow field. The half-width of the profile is about 4 frames/cycle, which indicates that a spectrum of frequencies is present. The large-scale puffing phenomenon is not perfectly periodic. There is no forcing function at the dominant frequency; effects like turbulence and slight variations in the boundary conditions due to air currents generated by the buoyant fire itself can cause the generation of vortices with irregular periodicity in this real system.

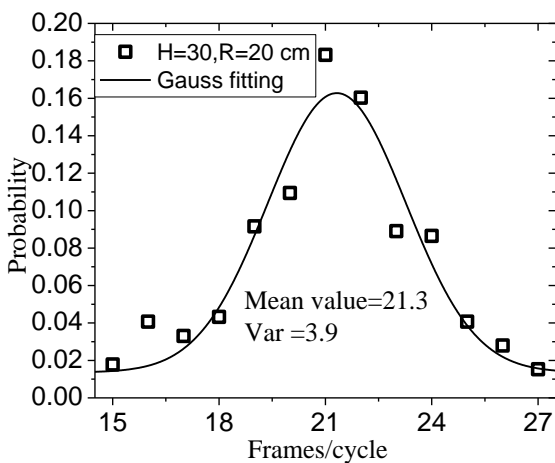


Figure 5 Normalized probability distribution of the period of the fire's puffing frequency

Figure 6 shows the fractional probability (P) of non-zero filament grayscale intensity (see Figure 4) as a function of location on each of the filaments. The largest values of P (=0.62) occurred at the centerline at H = 30 cm and 40 cm. The distribution was approximately symmetrical at all flame heights. The filaments lower in the flame (H=5 cm, 10 cm, 20 cm) had “M” shaped, double peaks with a minimum at the centerline, consistent with the structure of the fuel rich core immediately above the fuel surface. At H = 30 cm, the double peaks disappear and one maxima is apparent about the fire centerline.

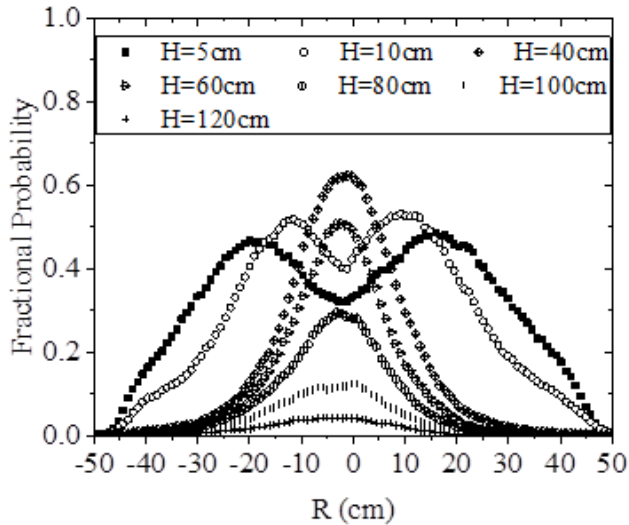


Figure 6 The probability of non-zero grayscale intensity as a function of radial location on the filaments

Figure 7 shows the calibration developed by considering the PDFs of the time series of corrected gas temperatures and the TFP grayscale pixel intensities at several fire locations (see Figure 2). For calibration, the PDFs of the time series of local filament intensity and the time series of corrected gas temperature were broken into 200 bins, with the average of each of the bins used to construct the calibration curve. As seen in Figure 7, the maximum, instantaneous, local, TC temperature was calculated to be as large as about 2350 K. There were very few instances that were measured to be so hot. It was at these moments when the filament signal was relatively strong, whereas when the filaments were below 1200 K, a much smaller intensity was emitted by the filaments. Thus, the nature of the experiments was such that the correlation between intensity and temperature was superior when P was larger (see Figure 6). To improve measurement accuracy, the analysis split the calibration into two pieces - P greater than or less than 0.46. Calibration curves were developed depending on the value of the fractional probability (P) (see Figure 6), which served to reduce measurement uncertainty.

Best fit curves shown in Figure 7 were created to correlate the data using an exponential of the form: $T \approx \exp(a-b/(I+c))$, where I is the filament grayscale pixel intensity and T is the gas flame temperature measured by the thermocouple and corrected for radiative loss and thermal inertia effects.^{99,10}

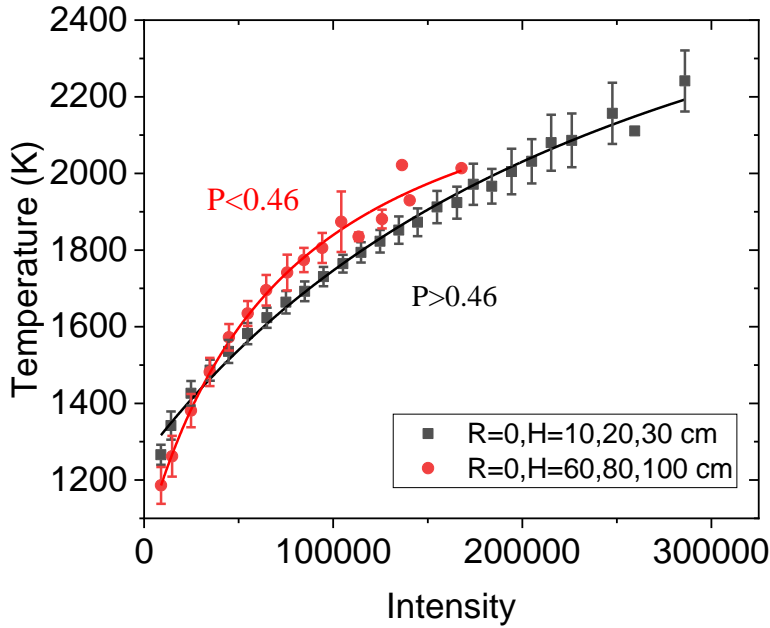


Figure 7 The averaged corrected gas temperature as a function of the grayscale filament intensity at several flame positions.

3.2 Local Temperature Distribution

Several approaches have been previously employed to interpret the TFP signal. A key challenge is to determine an accurate temperature when a large portion of the signal is too small to measure. Only considering instances when the filament signal is strong over-estimates the flame temperature, depending on the value of P .⁸ If $P=1$, this approach is reasonable, but Figure 8 shows that $P < 0.63$ at all locations. Assuming $T=300$ K when the instantaneous TFP signal is negligible under-estimates the local time-averaged temperature.⁸ Wang et al.⁸ assumed a Gaussian distribution for the temperature time series PDF at every location in a 0.30 m methanol pool fire and conducted a regression analysis to determine the mean and standard deviation. Here, a similar approach is taken, but the Beta function is selected, which handles the observed skewness in the PDF distributions, yielding a better goodness to fit than a simple Gaussian (with average R^2 values of 0.95 and 0.88 for Beta function and Gaussian fits to the TC data, respectively). The Beta function is defined as:¹⁹

$$B(\alpha, \beta) = \frac{\Gamma(\alpha+\beta)}{\Gamma(\alpha)\Gamma(\beta)} \quad (1)$$

where Γ is the Gamma function and α and β are fitting parameters. The mean and standard deviation of the Beta function distribution is:

$$\mu_{\bar{T}} = \frac{\alpha}{\alpha+\beta} \quad \text{and} \quad \sigma_{\bar{T}} = \frac{\alpha\beta}{(\alpha+\beta)^2(\alpha+\beta+1)} \quad (2)$$

For convenience, the temperature is normalized by the instantaneous measured temperature extremes, such that: $\bar{T} = \frac{T-300}{2350-300}$. A typical example is seen in Figure 8 (left), which compares Gaussian and Beta function fits of the dimensionless temperature at $H=100$ cm and $R=0$ cm. Figure 8 (right) shows how the local corrected TC distributions shift with distance above the burner (on the centerline) with the highest temperatures and broadest distributions near the burner surface. A perfect Gaussian is recovered when $\alpha = \beta$, which nearly occurs at $H=60$ cm (see Figure 8 right).

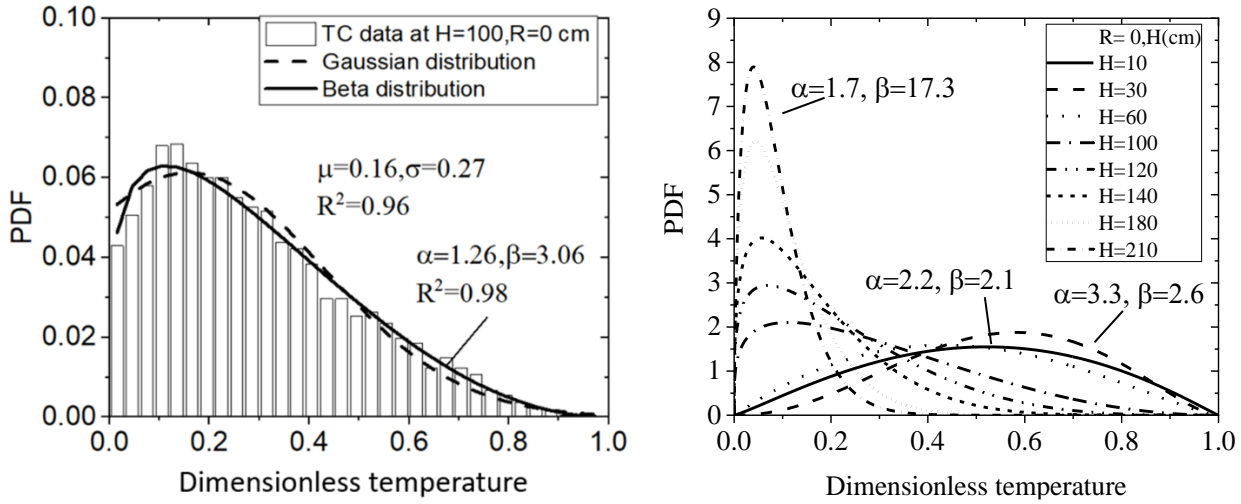


Figure 8 (left) Comparison of Gaussian and Beta function fits to the corrected dimensionless TC data at H=100cm, R=0 cm; (right) Dimensionless temperature distribution for locations along the fire centerline.

Figure 9 shows the correspondence between the normalized TFP gas temperature and the corrected TC PDFs of gas temperature at H=30 cm above the burner centerline. The cumulative distribution function (CDF) of the local, corrected, TFP gas temperatures was used to fit the data sets to a Beta function using a standard regression analysis in MATLAB. The non-dimensional mean temperatures were equal to 0.61 for both distributions, whereas the standard deviations were 0.015 and 0.017 for the TFP and TC distributions, respectively. CDF fits were obtained at all fire locations.

The largest contributors to the uncertainty of the instantaneous TFP temperature measurement was uncertainty in the thermocouple measurement, which was the basis of the calibration. A full propagation of error analysis shows that the relative standard uncertainty of the TFP temperature is between 90 K to 106 K (between 5 % to 6 %) for temperatures between 1400 K and 2100 K, respectively.

As described above, the mean temperature is determined by fitting the CDF to a Beta function. The uncertainty associated with the fitting routine to determine the local mean temperature ($\Delta\mu_{\bar{T}}$) is relatively small and approximately equal to $\sigma_{\bar{T}}/(PN)^{0.5}$, where N is the number of data instances (9000 frames)²⁰ and the observed values of P are given in Figure 6. The contribution to the uncertainty of the fitting routine is largest when P is small and is equal to about 2 K on-average and always less than 6 K.

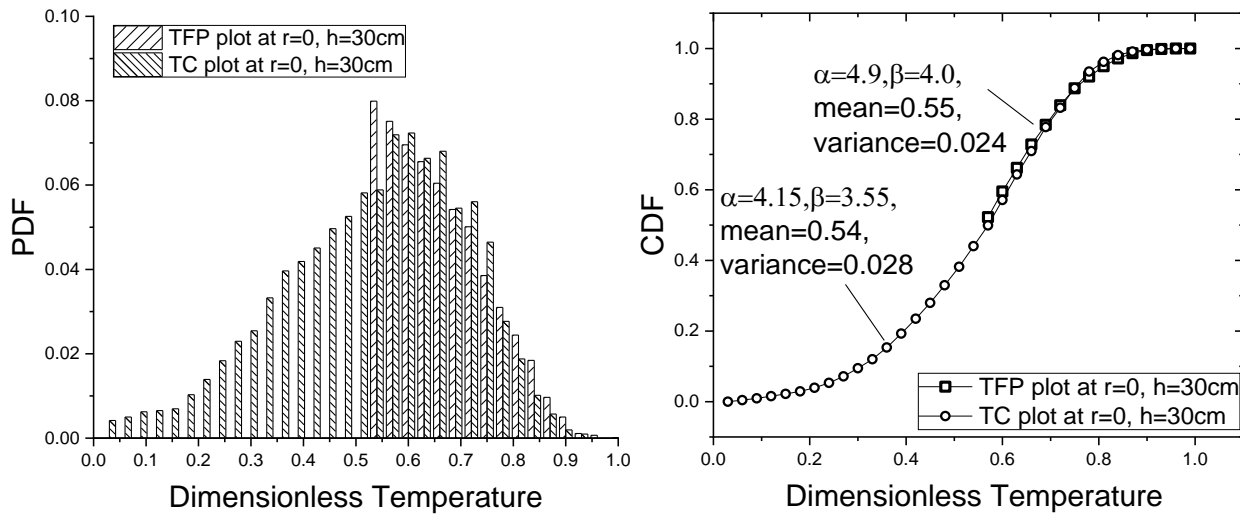


Figure 9 (left) PDFs and (right) CDFs of the TFP and TC temperatures at H=30cm above the burner centerline.

Figure 10 compares the mean TFP and TC temperature and variance as a function of distance above the burner. Although the trends in the CDF results were in general agreement with the trends in the corrected thermocouple measurements, the differences are greatest for the lower temperature regions, where low P values occur and a smaller number of occurrences are used to fit the temperature distribution.

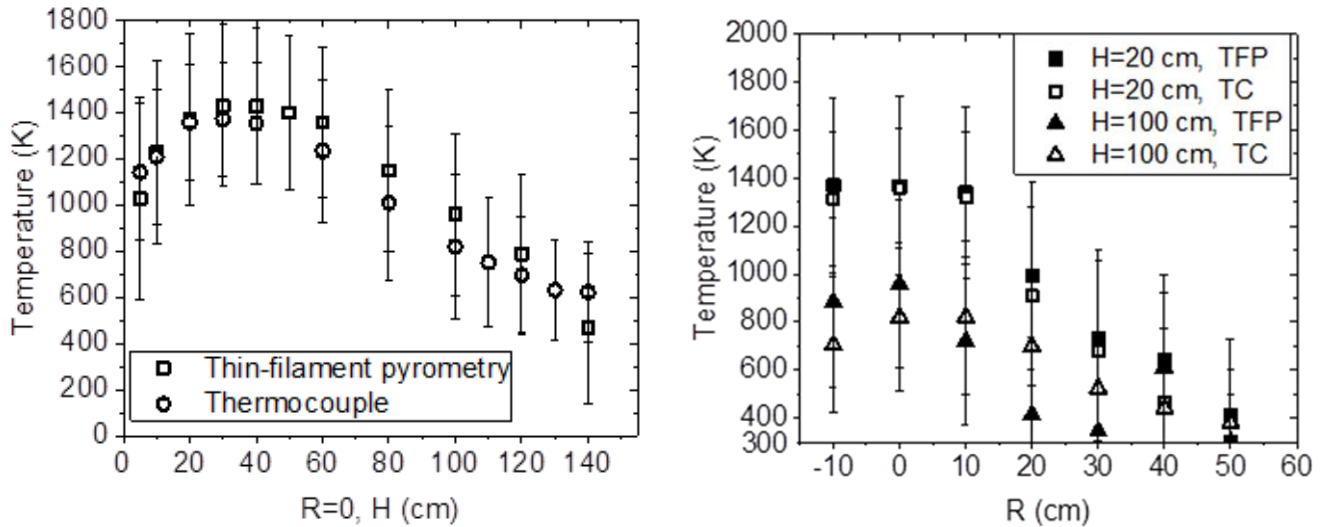


Figure 10. Comparison of the mean TFP and corrected TC gas temperatures as a function of vertical distance above the burner (H) along the centerline (left) and as a function of radial distance (R) from the pool center at various heights above the burner.

3.3 Temperature Field

False color maps of the field temperature were constructed using the time series of filament grayscale intensity. The maps provide a means to visualize the changing nature of the time-varying temperature field in the fire. Selection of the reference phases was based on identification of a moment in the cycle that was distinct, here taken as the frame with the tallest fire in a puffing cycle. The reference phase was independently determined for every

puffing cycle. Once selected, the frame order was defined for subsequent phases within that cycle (and that cycle only). The precise definition of the reference phase has no impact on this analysis, but is important for synchronization of the phases in the cycles. The maps were generated using linear interpolation between measurements. Interpolation in the vertical direction was based on distance between filaments (which varied with position), whereas interpolation in the radial (horizontal) direction was about every 2 mm.

The top left image in Figure 11 shows a false color map of mean temperature averaging all 9000 frames over the field. The rest of the images in Figure 11 represent false color maps of the average temperature field during each of five sequential phases during a single puffing cycle. Phase 1 represents the reference phase. Since the period of a puffing cycle is about 0.72 s on-average, the images are separated by about 0.14 s. To obtain these images, the time series of the measured TFP gas temperature field is transformed into “phase space.” Figure 11 represents all the data which includes puffing cycles of various duration (see Figure 5), so the temperature results were weighted using the distribution seen in Figure 5. The results were also normalized, assuming that the temperature at each point in the field was approximately linear in time from frame to frame (0.033 s).

Although this is a relatively slowly-puffing fire - with a characteristic puffing period of about 0.730 s, turbulent fluctuations on the order of 200 Hz can be expected within this buoyancy dominated fire. The TFP method, with a time response on the order of 3 ms, can be expected to easily resolve the dominant puffing frequency and a significant fraction of the natural temperature fluctuations. There is some smearing, or averaging, of the instantaneous temperature field due to the measurement system time response.⁵ For example, the temperature field data are averaged over the duration of the camera shutter opening time, which is 60 Hz or 17 ms in duration. Uncertainty in the selection of the reference phase of the cycles (i.e., the exact duration of the puffing period and the offset of the initial phase of the reference frames relative to the video record) also contributes to temporal smearing of the temperature field. These issues lead to an estimated uncertainty of ½ frame (9 ms) and 1 frame (17 ms), respectively, in the measured period of a cycle. The combination of these variances represents about $\sqrt{3/2}$ frames (or 0.040 s). For a 21 frame puffing cycle, this represents about a 6 % temporal uncertainty. Unresolved, fast, turbulent fluctuations also contribute to smearing of the temperature field.

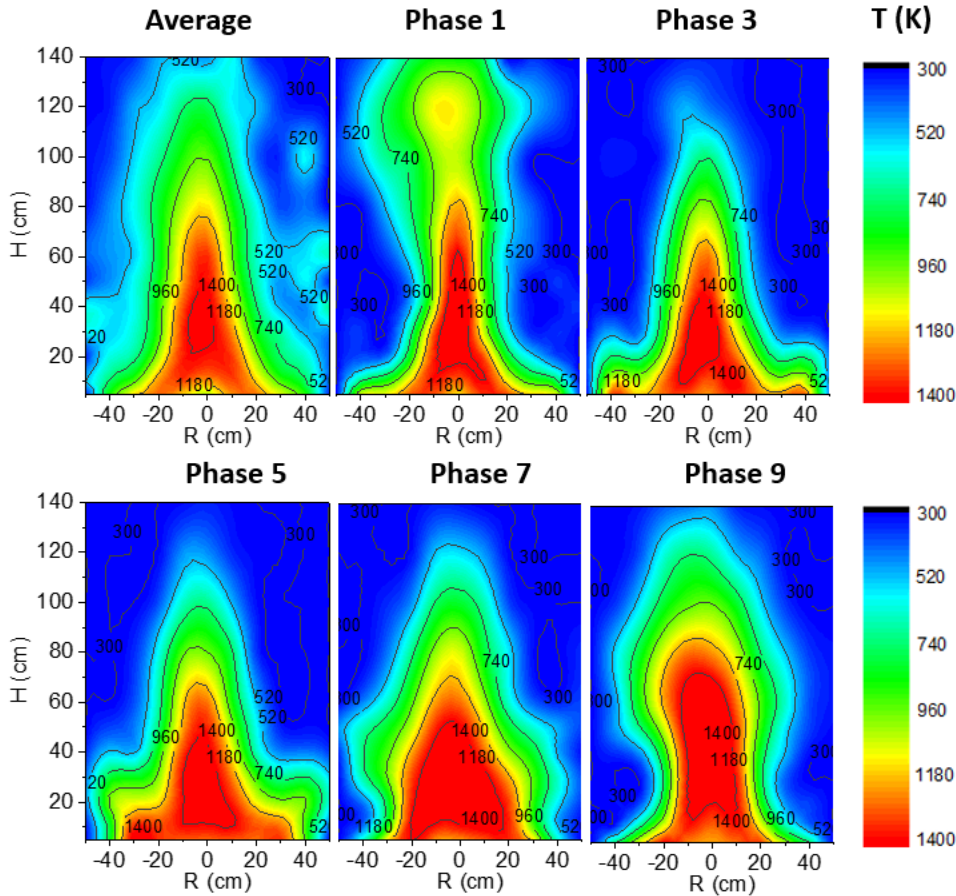


Figure 11 False color maps of the temperature field in a plane through the fire centerline, including the time-averaged temperature field (top left) and the average temperature fields during five phases of a 10 phase puffing cycle.

Figure 11 reveals the evolving temperature field during the puffing cycle of the 1 m methanol pool fire. The temperature of the inner core remains about the same but its extent and the outer portion of the fire is characterized by the motion of a bulge that travels upwards. This is consistent with the appearance of the visible fire. The bulge is associated with generation of toroidal vortices rolling into the fire plume as the entraining fluid encounters large density gradients.²¹ These same large-scale features are present in the pulsing 30 cm methanol pool fire.⁸ At any one location, the value of the temperature gradient changes as the fire undergoes its puffing cycle. The pulsing fire exhibits larger temperature gradients in the horizontal direction than the vertical, with values as large as 80 K/cm at 30 cm above the burner, for example, during Phase 9 in Figure 11. The time-averaged field in Figure 11 (top left) obscures the complexities of the pulsing fire behavior and smears the thermal field.

4. SUMMARY AND CONCLUSIONS

Measurements were conducted to characterize the transient temperature field in a 1 m methanol pool fire steadily burning in a quiescent environment. A correlation was developed between measurements of the probability

density functions of corrected thermocouple temperatures and filament luminosities. A regression analysis of the TFP results using the cumulative density function associated with a Beta function yields the mean temperature and its variance as a function of location. Use of a Beta function rather than a Gaussian improves the characterization of the local temperature and its variance. The approach fully exploits the high temperature filament intensity information, rather than assuming that negligible filament intensity implies a temperature of 300 K. Further analysis considers the cyclic nature of the puffing fire by transforming the time series of field temperatures into “phase space.” This allows quantification of the evolving temperature field during a puffing cycle with a relative standard uncertainty of the local temperature on the order of 100 K. The method does better in the high temperature regions of the fire, where the filament intensity is relatively large. Future studies may wish to consider use of a second camera, synchronized and set to a higher sensitivity that may be able to effectively stretch the dynamic range of the temperature measurement by simultaneously capturing lower temperature filament emission.

The results of the study provide quantitative insight into the complex structure and dynamics of a large diameter pool fire and provide a unique data set for validation of CFD fire models. To compare measurements with simulations, the simulations must follow the same processing recipe as the temperature field determination used here, which includes consistent selection of a reference phase for each and every puffing cycle, cutting the puffing cycle into ten phases, and appropriately averaging the temperature field. Such a comparison would provide a more rigorous test of the dynamics of a CFD fire model than simple checks of the time-averaged temperature field. Consideration of only time-averaged temperatures omits consideration of detailed information on the spatial extent and temporal character of important fire features such as the high temperature reaction zone as it waves back and forth in the puffing fire.

5. ACKNOWLEDGEMENTS

Then authors are grateful to Matt Bundy for extremely helpful discussions and support in the conduct of the experiments and to Marco Fernandez for excellent technical support.

6. REFERENCES

1. Joulain P, The Behavior of Pool Fires: State of the Art and New Insights, *Proc Combust Inst* 1998, 27: 2691-2706.
2. Hu, L, A Review of Physics and Correlations of Pool Fire Behaviour in Wind and Future Challenges, *Fire Safety J* 2017, 91:41-55. <https://doi.org/10.1016/j.firesaf.2017.05.008>
3. Liu J, Li J, Fan C, A bibliometric study of pool fire related publications, *J Loss Prevention Process Industries*, 63, 2020, 104030, <https://doi.org/10.1016/j.jlp.2019.104030>.
4. Vilimpoc, V, Goss, LP, SiC-Based Thin-Filament Pyrometry: Theory and Thermal Properties, *Proc Combust Inst* 1988, 22: 1907-1914.
5. Hariharan SB, Sluder ET, Gollner, MJ, Oran, ES. Thermal Structure of the Blue Whirl, *Proc Combust Inst* 2019, 37: 4285-4293.
6. Hariharan, SB. The Structure of the Blue Whirl: A Soot-Free Reacting Vortex Phenomenon, *Master's Thesis*, University of Maryland at College Park, 2017.
7. Pitts WM. Thin Filament Pyrometry in Flickering Diffusion Flames, *Proc Combust Inst* 1996, 26: 1171-1179.
8. Wang Z, Tam WC, Chen J, et al. Thin Filament Pyrometry Field Measurements in a Medium-Scale Pool Fire, *Fire Technology* 2019, 56:837-861. <https://doi.org/10.1007/s10694-019-00906-9>
9. Sung K, Chen J, Bundy M, Hamins A. The Characteristics of a 1 m Methanol Pool Fire, *Fire Safety J* 120: 2021 103121, available on-line: <https://doi.org/10.1016/j.firesaf.2020.103121>

-
10. Sung K, Chen J, Bundy M, et al., The Thermal Character of a 1 m Methanol Pool Fire, *NIST Technical Note 2083*, National Institute of Standards and Technology, Gaithersburg, MD, Feb. 2020.
<https://doi.org/10.6028/NIST.TN.2083>
 11. Shaddix, C. R, Correcting Thermocouple Measurements for Radiation Loss: A Critical Review, American Society of Mechanical Engineers, New York, NY (US); Sandia National Labs., Livermore, CA (US), 1999.
 12. Jaeger FM, Rosenbohm E. The Exact Formulae for the True and Mean Specific Heats of Platinum, *Physica* 1939, 1123-1125.
 13. McGrattan K, Hostikka S, Floyd J, et al. Fire Dynamics Simulator, Sixth Edition, *NIST Special Publication 1019*, National Institute of Standards and Technology, Gaithersburg, MD, 2020.
 14. Hurley M (Ed.). *SFPE Handbook of Fire Protection Engineering*, 5th ed., Society of Fire Protection Engineers, 2016, Chapter 13.
 15. Ichikawa H. Advances in SiC Fibers for High Temperature Applications, *Advances in Science and Technology Online* 2006, 50:17-23.
 16. Maun JD, Sunderland PB, Urban DL. Thin-filament pyrometry with a digital still camera, *Applied Optics* 2007, 46: 483-488.
 17. Bedat, B, Giovanni A, Pautin S. Thin Filament Infrared Pyrometry: Instantaneous Temperature Profile Measurements in a Weakly Turbulent Hydrocarbon Premixed Flame, *Experiments in. Fluids* 1994, 17: 397-404.
 18. Mathworks Documentation: rgb2gray; website consulted 7/1/2018
<https://www.mathworks.com/help/matlab/ref/rgb2gray.html>
 19. Peters N. *Turbulent Combustion*, Cambridge University Press, Cambridge, U.K., 2000, p. 197.
 20. Rice, JA. *Mathematical Statistics and Data Analysis* (3rd ed.), Thomson Higher Education, Belmont, CA, USA (2007) p. 255.
 21. Baum HR, McCaffrey BJ. Fire Induced Flow Field – Theory and Experiment, *Fire Safety Science* 1989, 2: 129-148.